ADVANCED MATERIALS INTERFACES
www.advmatinterfaces.de

Formation of Flat-on Lamellar Crystals in Absence of Nanoconfinement

Liangyong Chu, Wouter J. B. Grouve, Martin van Drongelen, Erik G. de Vries, Remko Akkerman, and Matthijn B. de Rooij**

Flat-on lamellar crystals are crucial for gas-barrier polymer films. The formation of this lamellar crystalline structure with chains perpendicular to the substrate is currently understood as the result of confined crystallization, e.g., in block copolymers and ultrathin polymer films. In this paper, it is demonstrated that these flat-on lamellar crystals of various thermoplastic polymers may form on stainless steel and silicon wafer surfaces without the presence of confined crystallization. Atomic force microscopy, high-resolution scanning electron microscopy, and polarized light hot-stage microscopy are used to characterize the formation of the lamellar crystals. Further results show that the surface physicochemical properties of the substrates strongly influence the formation of these lamellar crystals. A hypothesis, based on the heterogeneous crystallization theory, is proposed to explain the formation of such flat-on lamellar crystals. These results are crucial for a fundamental understanding of the formation of lamellar crystals and may provide a new approach to fabricate such structures.

In semicrystalline polymers, chains can tightly pack and fold back and forth into crystalline lamellae. This lamella is the fundamental structure of 3D larger scale assemblies, such as sheaves and spherulites.[1] Under the right conditions, a lamellar crystal can form, with chains perpendicular to the substrate (flat-on lamella), as shown in **Figure 1**.[2]

The flat-on lamellar structure is crucial for many engineering applications of polymers, such as gas-barrier polymer films as used in food, medicine, and electronic packaging, and metal-polymer joints as used in automotive and aerospace engineering where moisture adsorption at the interface plays an important role in the long-term joint performance.[3,4] This is because the flat-on lamellar structures help to significantly reduce the diffusion rate of small molecules, e.g., oxygen and moisture, due to their unique structure, with tightly packed polymer chains oriented perpendicular to the substrate.

The formation of the flat-on lamellar crystalline structures is currently understood as the result of confined crystallization.[5] Two types of confined crystallization have been reported. The first type has been found when microphase-separation occurs, e.g., in block copolymers or polymer blends. When the crystallization temperature (T_c) of each component is different, the component with a higher T_c crystallizes first and forms a nano- or microscale confinement for the other polymer. Thus, the component with a lower T_c crystalizes under confinement.[6] The second type of confined crystallization has been found in ultrathin films from dilute polymer solutions or polymer melts.[7] This lamellar crystalline structure has been found in various crystalline polymers, such as poly(vinylidene fluoride), poly(ethylene oxide), poly(3-hydroxybutyrate), and poly(l-lactide).[8] Although the crystallization mechanisms for the formation of these lamellar crystalline structures, e.g., regarding growth orientation, are still not well understood, the nanoscale confinement (with an order of few tens of nanometers) is considered as the key for the formation of these lamellar crystalline structures.

In our previous paper, on the influence of the polymer interphase structure on the adhesion between a semicrystalline thermoplastic and a metal, we showed that a lamellar structure can be found at the polymer-metal interphase.[9] The formation of the lamellar structure has a significant influence on the fracture behavior of the metal-thermoplastic interface, which is crucial in, for example, the release of thermoplastics from mold surfaces. These results indicate that a lamellar crystalline structure may form without the aforementioned nanoscale confinement. In this paper, the lamellar crystalline structure at the polymer interphase is further studied for various semicrystalline thermoplastics and different substrate materials. The role of surface physical properties of the substrate on the formation of this lamellar structure is also studied by using a silicon

Dr. L. Chu, Dr. W. J. B. Grouve, Dr. M. van Drongelen, E. G. de Vries, Prof. R. Akkerman, Prof. M. B. de Rooij
Department of Mechanics of Solids
Surface and Systems
Faculty of Engineering Technology
University of Twente
Enschede 7500AE, The Netherlands
E-mail: l.chu@utwente.nl; m.b.derooij@utwente.nl
Prof. R. Akkerman
ThermoPlastic composites Research Center (TPRC)
Palatijn 15, Enschede 7521PN, The Netherlands
The ORCID identification number(s) for the author(s) of this article can be found under https://doi.org/10.1002/admi.202001894.

DOI: 10.1002/admi.202001894

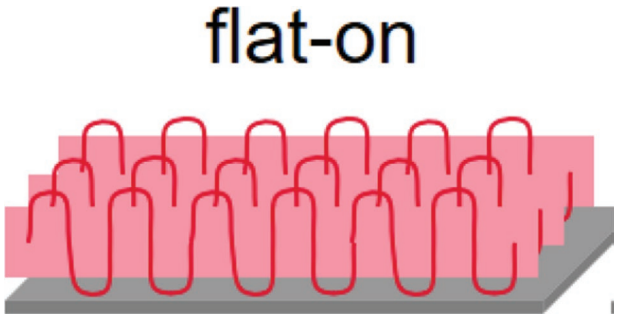

Figure 1. Schematic drawing of the flat-on lamella.

wafer and a graphene-coated surface. A hypothesis is proposed to explain the formation of the lamellar structure by taking into account the role of surface physicochemical properties including surface chemical composition and lattice parameters. These results help the fundamental understanding of the formation of lamellar structures and may give a guide to the development of a new methodology to prepare such 2D structures.

Experimental Section

Materials: Four different polymers are studied in this work, namely

- Poly(ether ketone ketone) (PEKK) known as Kepstan 8000, from Arkema in the form of film.
- Poly(ether ether ketone) (PEEK), known as Victrex 150P, from Victrex in the form of powder.
- Poly(phenylene sulfide) (PPS), known as Fortron 0214, from Celanese in the form of film.
- Polyamide 6 (PA-6), known as AM306300 as bought from Goodfellow in the form of powder.
- Besides the polymers, the following substrates were considered:
- AISI 430 stainless steel sheets as supplied by Metaalketen.
- A graphene-coated silicon wafer was purchased from Graphene Supermarket.
- Highly ordered pyrolytic graphite (HOPG) was obtained from Sigma-Aldrich.
- A (100) Silicon wafer with a native oxide layer of about 2 nm obtained from Sil'Tronix Silicon Technologies.

Characterization and Sample Preparation—Characterization: The atomic force microscopy (AFM) morphology characterization is performed using a Park XE-100 AFM from Park Systems using an ACTA AFM probe purchased from AppNano. The spring constant of the probe is 26 N m^{-1} determined using the thermal noise method.[10]

A Sensofar S Neox confocal microscopy is used for all the optical microscopy characterizations. A ZEISS MERLIN scanning electron microscope (SEM) was used to characterize the surface morphology of the crystalized PEKK surface and the cross-section of the PEKK film. All the SEM characterizations are operated at 1 kV.

A THMS600 hot-stage, purchased from Linkam Scientific Instruments, is used in conjunction with a VHX-6000 polarized light digital microscope from KEYENCE Corporation, to characterize the crystal growth at the contact with a graphene-coated surface.

Characterization and Sample Preparation—Sample Preparation: Polymer Residual on the Substrate: Sample preparation involves the following steps. First, a thermoplastic film is sandwiched between two substrates, e.g., two stainless steel sheets. Subsequently, the samples are placed in an oven, melted for 5 min (380 °C for PEKK and PEEK, 320 °C for PPS, and 250 °C for PA-6), and then naturally cooled down to room temperature at a rate of ≈0.5 °C min^{-1}. Then, the sandwich is mechanically opened to provide the two substrates partially covered with residual polymer. A detailed description of the separation procedure can be found in our previous paper.[9] Due to its brittleness, a slightly different procedure was followed for the silicon wafer. Here, a steel-PEKK-Si sandwich is first prepared. To open the sandwich, another stainless steel plate is then adhesively bonded on the backside of the silicon wafer, after which it can be opened. Despite the precautions, the silicon wafer still breaks during the debonding because of the strong adhesion force between the PEKK and the silicon surface. The preparation of the sample with PEKK residual on a silicon wafer is schematically shown in **Figure 2**.

Characterization and Sample Preparation—Sample Preparation: Crystalline (Spherulitic) Substrates: To prepare the crystallized PEKK and PA-6 samples, used to characterize the lamellar crystal thickness in a spherulite by means of AFM, a 1 cm x 1 cm thermoplastic film with a thickness of 50 µm is placed on a stainless steel substrate in a vacuum oven. After melting (380 °C for PEKK and 250 °C for PA-6) for 5 min, the film is cooled down and crystallized at a rate of 0.5 °C min^{-1} inside the vacuum oven.

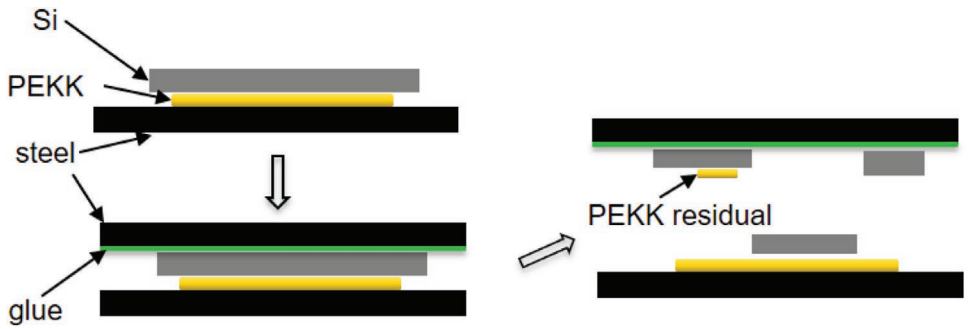

Figure 2. Schematic drawing of the preparation of the sample with PEKK residual on a silicon wafer.

Characterization and Sample Preparation—Sample Preparation: PEKK Films for SEM Characterization: Two PEKK films were prepared for SEM characterization

- A 1 cm x 1 cm PEKK film with a thickness of 50 µm was placed on a stainless steel substrate inside an oven. The other side was exposed to air. After melting at 380 °C for 5 min, the film and substrate were cooled down at the rate of 0.5 °C min^{-1}; the thermal treatment was the same as used to prepare the steel—PEKK—steel sandwich. Afterward, the stainless steel was chemically etched away using a 250 mL H_2SO_4 solution (4 mol L^{-1} H_2SO_4 solution, 98.0 wt% Sulfuric acid purchased from Sigma-Aldrich). Subsequently, the PEKK film was bent until it breaks using two tweezers to obtain information on the crystalline structure in the cross-section using microscopy.
- A 1 cm x 1 cm PEKK film with a thickness of 50 µm was placed on the graphene-coated silicon wafer surface. The thermal treatment of the sample was the same as the first sample. After cooling, the PEKK film was released from the graphene-coated surface using a tweezer. Again, the PEKK film was bent until it breaks to allow microscopy on the cross-section to study the crystalline structure.

Characterization and Sample Preparation—Sample Preparation: Hot-Stage Polarized Light Microscopy Characterization: The surface of a piece of graphite flake, mechanically exfoliated from the highly oriented pyrolytic graphite (HOPG) using scotch tape, was used to represent a graphene-coated surface. As schematically shown in **Figure 3**, the graphite flake composed of multilayer graphene is folded and then used in hot-stage experiments. During the experiments, the folded graphite flake and the thermoplastic film were put on top of a transparent glass plate. Next, the sample was heated up to 400 °C at a rate of 40 °C min^{-1}. After annealing for 5 min to remove all the PEKK crystals, the system cools down to 315 °C at a rate of 20 °C min^{-1}. Polarized light microscopy was then used to study the formation of the crystalline structure.

The height morphology of the thermoplastic residual layer on the stainless steel substrates, after the opening of the sandwich joint, is shown in **Figure 4**. Four types of thermoplastics including PEKK, PEEK, PPS, and PA-6 were used. (PEKK on stainless steel has been published in our previous paper and is not included here).[9] The first column shows the obtained results for PPS. Figure 4a shows the optical image of the PPS residual on the stainless steel surface. The polymer layer is recognized on the substrate and can be distinguished by the difference in brightness. Figure 4b shows the height morphology of the area marked by the red square in Figure 4a as characterized using AFM. The height profile along the dashed line in Figure 4b is shown in Figure 4c. The height peaks at the beginning and end of the scanned lines are probably due to the pulling force applied to the film during the separation of the metal-thermoplastic joint. The thickness of the PPS residual film is about 30 nm. The characterization of the polymer film structure of PEEK and PA-6, including the optical images and AFM height characterizations, are shown in Figure 4d–f,g–i, respectively. The thickness of the PEEK and PA-6 lamella is characterized as 20 and 40 nm, respectively. The thickness of the PEKK layer is characterized as 20 nm as published in our earlier work.[9] The results in Figure 4 show that when semicrystalline thermoplastics are melted and crystallized in contact with a stainless steel surface, a polymer layer structure is formed at the interface with the substrate. This polymer layer structure has a uniform thickness which varies between different types of thermoplastics. Results in our previous paper show that the formation of this layer structure influences the fracture behavior of the polymer-stainless steel interface. The bond strength between the polymer layer and the stainless steel substrate is stronger than the bond strength between the polymer layer and the bulk polymer.[9] Thus, fracture occurs at the interface between the polymer layer and the bulk polymer during the opening of the stainless steel-thermoplastic joint, hence, leaving a polymer residue on the substrate. Next, two characterization approaches as detailed in part 3.2 and 3.3 are used to make plausible that these polymer residual layers are, in fact, flat-on lamellar crystals.

As a first step in our approach to make plausible that these polymer residual layers are flat-on lamellar crystals, the thickness of the polymer residual layers is compared with the thickness of the lamellar crystals formed in spherulites.[11,13] A spherulite is composed of an assembly of many lamellar crystals as schematically shown in **Figure 5**a.[11,12] The surface of a spherulite is occupied by lamellar crystal regions and amorphous regions. Figure 5b shows the height morphology of the PA-6 surface from which the spherulites can be recognized. It is good to stress here that the sample was prepared using the same thermal treatment as the sample shown in Figure 4g. Figure 5c shows the high-resolution scan of the area marked in the red square in Figure 5b. Lamellar crystals are recognized with a thickness of 40 nm. This thickness is the same as the PA-6 residual layer as shown in Figure 4g–i.

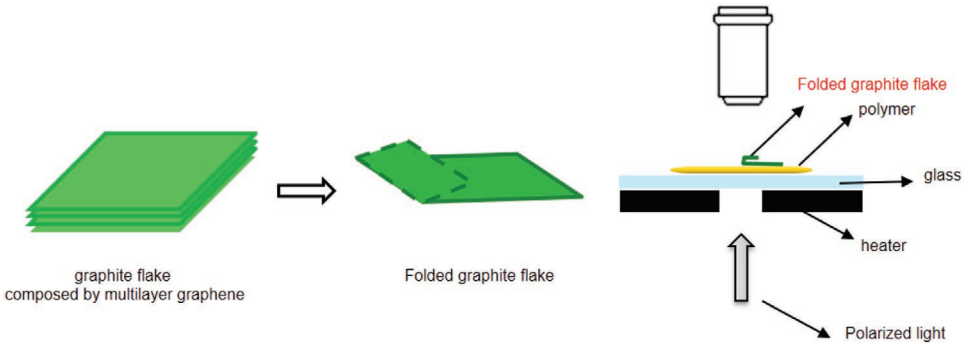

Figure 3. Schematic drawing of using folded graphite flake in the polarized light hot-stage microscopy.

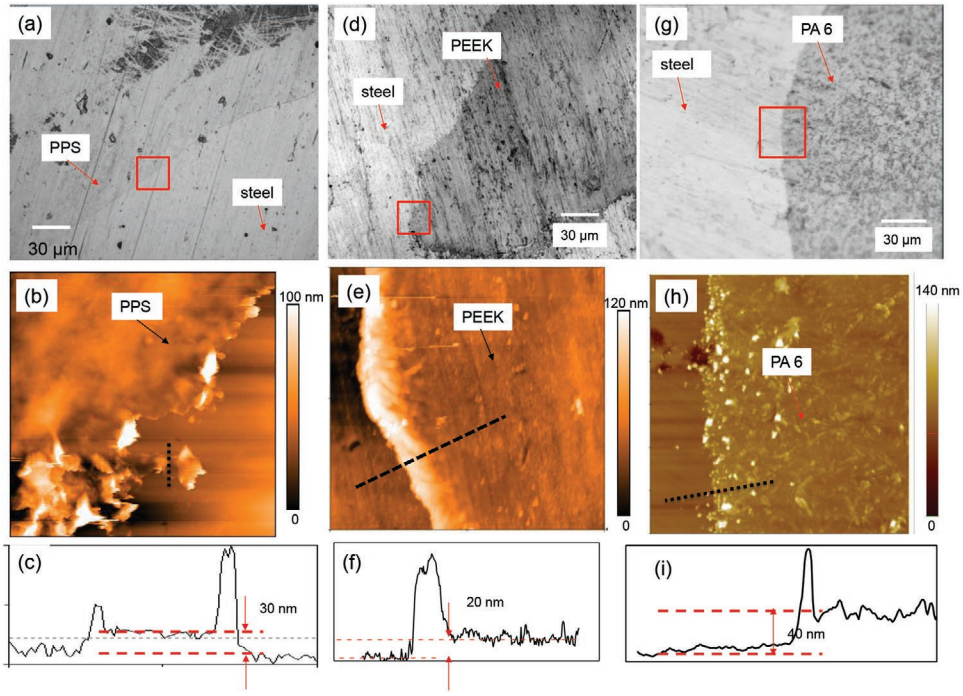

Figure 4. Optical images of the PPS a), PEEK d), and PA-6 g) residual on the stainless steel substrate. AFM height image of the PPS b), PEEK e), and PA-6 h) structure of the areas marked as the red square in a), d), and g), respectively. c), f), and i) show height profiles along the dark line in b), e), and h), respectively.

Figure 5d shows the height morphology of the PEKK surface, characterized using AFM. Again, the sample was prepared using the same thermal treatment as the sandwich specimens discussed in the previous section. Also here, the PEKK spherulites are recognized on the surface. Figure 5e shows the high-resolution scan of the area marked in the red square in Figure 5b.

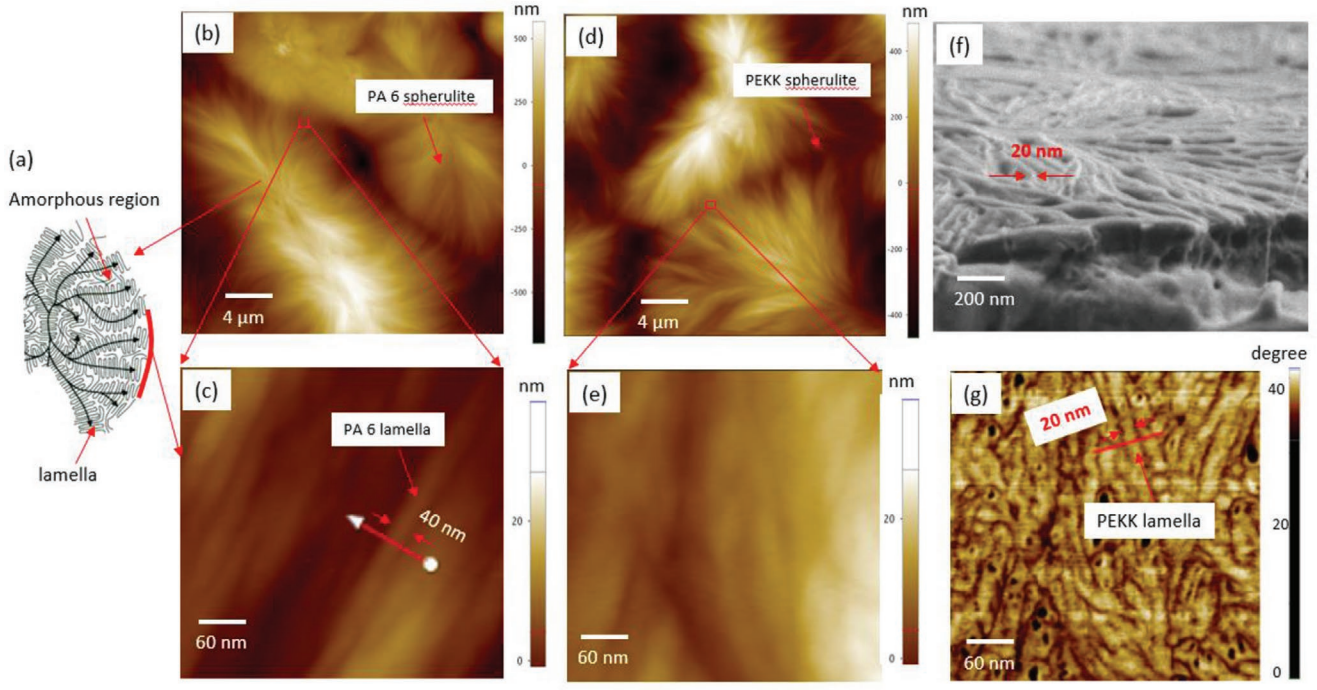

Figure 5. a) Schematic drawing of a spherulite.[11,12] b) AFM height morphology of the crystalized PA-6 surface wherein spherulites are recognized. c) High-resolution AFM height morphology of the area marked as the red square in b). d) AFM height morphology of the crystalized PEKK surface where spherulites are recognized. e) High-resolution AFM height morphology of the area marked as the red square in d). f) High-resolution SEM image of the crystalized PEKK surface. g) AFM phase image corresponding to subfigure e).

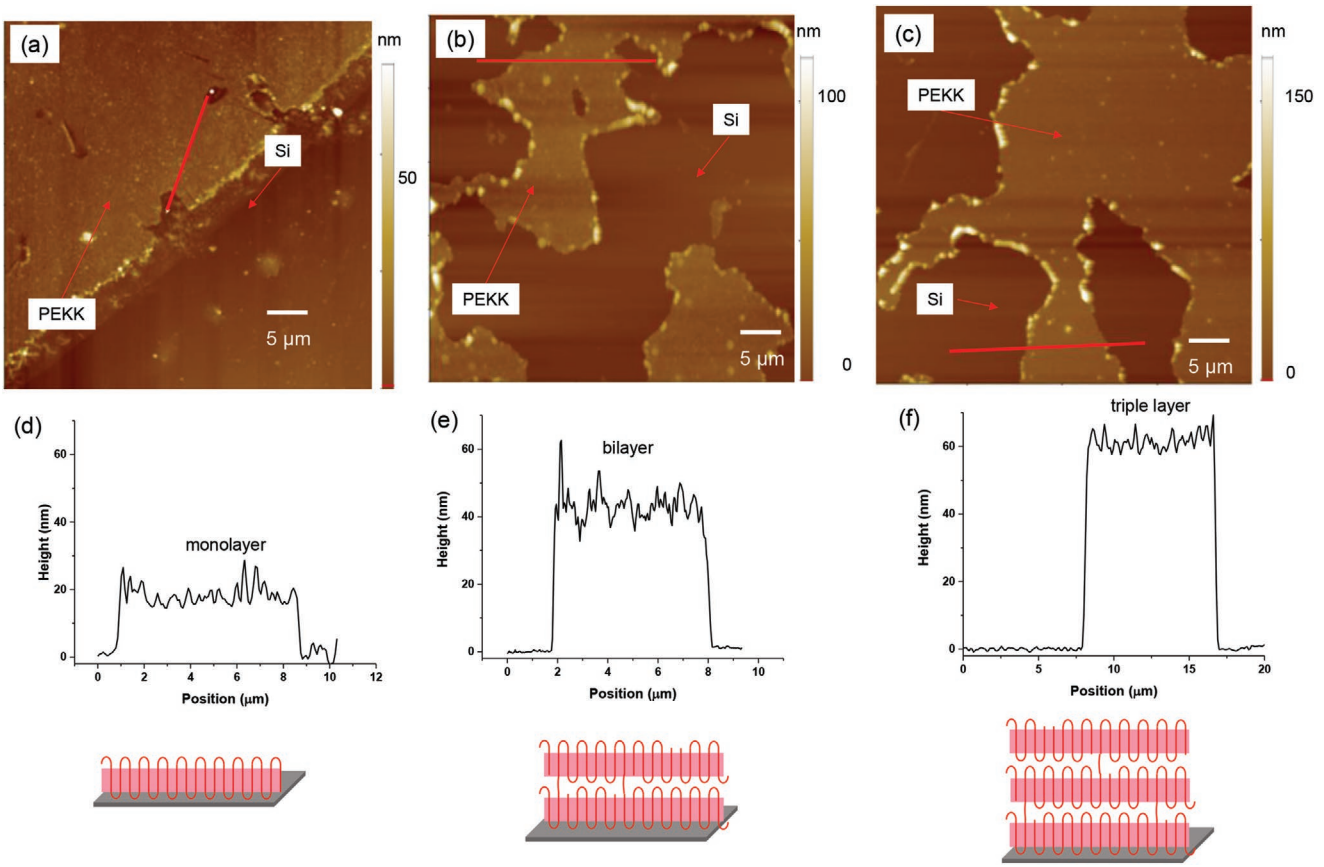

Figure 6. a) AFM height image of the PEKK residual layer on the silicon wafer surface. b) AFM height image of the PEKK residue layer on the silicon wafer surface in another area. c) AFM height image of the PEKK residue layer on the silicon wafer surface in a third area. d), e), and f) show height profiles along the red lines in a), b), and c), respectively.

The AFM phase image corresponding to Figure 5e is shown in Figure 5g. In an AFM phase image, the phase shift measured is proportional to the stiffness of the materials.[14] The PEKK lamellar crystalline regions and amorphous regions are recognized in the AFM phase image in Figure 5g. The thickness of the PEKK lamellar crystal is characterized as 20 nm. The PEKK spherulite surface was also characterized using the high-resolution SEM as shown in Figure 5f. The PEKK lamellar crystals can be distinguished and the thickness of the PEKK lamellar crystal is characterized as 20 nm. The thickness of a PEKK lamellar crystal as found in the PEKK spherulite is the same as the PEKK residual layer on the stainless steel surface. Though the lamellar thickness for a specific polymer varies depends on the processing conditions, the order of magnitude is the same.[15] It is concluded that the thermoplastics residual layer on a stainless steel substrate has the same thickness as lamellar crystals found in the thermoplastics spherulites. These results are consistent with the assumption that the layer as shown in Figure 4 consists out of the flat-on lamellar crystals with chains perpendicular to the substrate. In the next section, more evidence is gathered by examining multiple areas of the PEKK residual layer.

To further analyze the layer thickness for PEKK, an atomically smooth silicon wafer was used as a substrate. This allows accurate determination of the thickness of the polymer residual layer. **Figure 6**a shows the height morphology of the PEKK residual layer found on the silicon wafer characterized using AFM, while the height profile along the red line in Figure 6a is shown in Figure 6d. A uniform PEKK lamellar layer with a thickness of 20 nm is recognized, which is similar to the layer thickness observed for PEKK in contact with steel and similar to the PEKK lamellar crystal thickness. Figure 6b shows the height of the PEKK residual layer found in a different area. Here, a uniform PEKK lamellar layer with a thickness of about 40 nm is recognized, which is equal to twice the layer thickness observed for a PEKK lamellar crystal. Figures 6c shows the height morphology of the PEKK residual layer found on yet another location. A uniform PEKK lamellar layer with a thickness of about 60 nm is recognized, which is equal to three times the layer thickness observed for a PEKK lamellar crystal. The formation of uniform PEKK residual layers with the thickness of one, two, and three times the PEKK lamellar crystal thickness indicates that lamellar crystals form at the contact with the stainless steel and a silicon wafer surface.

The results, as shown in Figures 4–6, demonstrated that the flat-on thermoplastic lamellar crystals with chains perpendicular to the substrate form when molten thermoplastics crystallize in contact with both the stainless steel surface and the silicon wafer surface. The lamellar layer remained on these substrates after a brittle fracture with the main body of the polymer. As such, the formation of these flat-on lamellar crystals occurs without the presence of the nanoscale confinement.

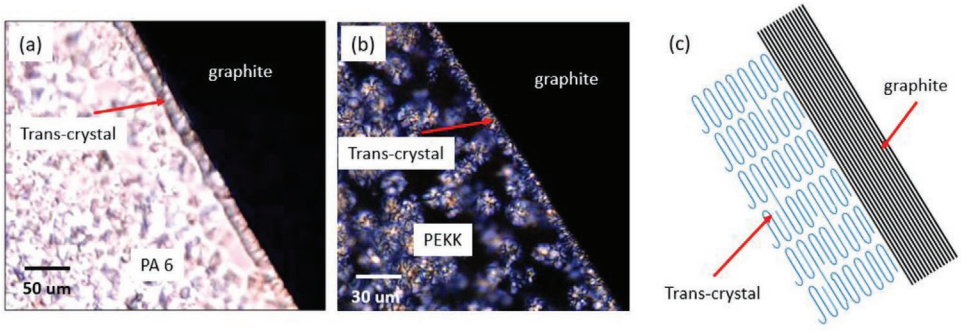

Figure 7. PA-6 a) and PEKK b) crystallized at the contact with a graphite surface characterized using hot-stage polarized light microscopy. c) Schematic drawing of the trans-crystalline structure formed at the contact with a graphite surface.

We hypothesize that this structure forms due to crystallization at the contact with the solid substrate surface. To further study the role of surface physicochemical properties on the formation of such a lamellar crystalline structure, graphite (graphene-coated) surface is further used as the substrate.

The crystalline structure at the contact with the graphite surface was studied for the different thermoplastics (PEKK and PA-6) using hot-stage polarized light microscopy. **Figure 7**a,b shows the formation of PA-6 and PEKK trans-crystalline structures at the contact with a graphite surface. Different from the flat-on lamellar crystals formed at the contact with stainless steel and Si surface, a trans-crystalline structure with crystal growth orientation perpendicular to the substrate was recognized (polymer chains are parallel to the substrate). The growths of crystals normal to the fiber surface is caused by a high nucleation density of polymers at the contact with the substrate surface, e.g., a carbon fiber.[16] A schematic drawing of the trans-crystalline structure is shown in Figure 7c.[16] Moreover, when a trans-crystalline structure forms at the polymer interphase, the thermoplastic film easily releases from the substrate which has been studied in our previous paper.[9]

Figure 8a shows the fracture surface of a PEKK film after release from a graphene-coated silicon wafer surface. The top bright part is the surface formed at the contact with graphene and the dark part is the cross-section of the film. A neat fracture surface is recognized, with a trans-crystalline structure, for the side which was in contact with the graphene. The fracture surface of a PEKK film formed at the contact with the stainless steel surface was also prepared after the stainless steel substrate was chemically etched away (more details can be found in the Experimental Section). The fracture surface of the polymer film with flat-on lamellar crystals on the surface is shown in Figure 8b,c. More deformation was recognized on the surface due to the presence of this lamellar crystal structure. The different fracture behavior of these two thermoplastic films is consistent with our argument that they have different polymer interphase structures.

All samples were prepared under the same thermal treatment and no efforts were taken to confine crystallization. Comparing all polymer/substrate combinations, the formation of a flat-on lamellar crystal with chains perpendicular to the substrate is probably due to the surface physicochemical properties of the substrates. Based on these results, a hypothesis is proposed using heterogeneous crystallization theories to further explain the formation mechanism of a lamellar crystal without the nanoscale confinement.

Figure 9 shows a schematic drawing of the formation of trans-crystalline (Figure 9a,b) and flat-on crystalline structures (Figure 9c) formed at the contact with the substrates. During the cooling of the thermoplastic melts, the polymer molecules fold back and forth to minimize the free energy. During crystallization, the total free energy of the system including both the polymer crystal and polymer-substrate interface needs to be minimized.[17] For a specific polymer, the free energy at the polymer-substrate interface is determined by the chemical composition of the substrate and atomic lattice matching between the polymer crystal and the substrate.[18] These surface physicochemical properties vary with different substrates.[19] For

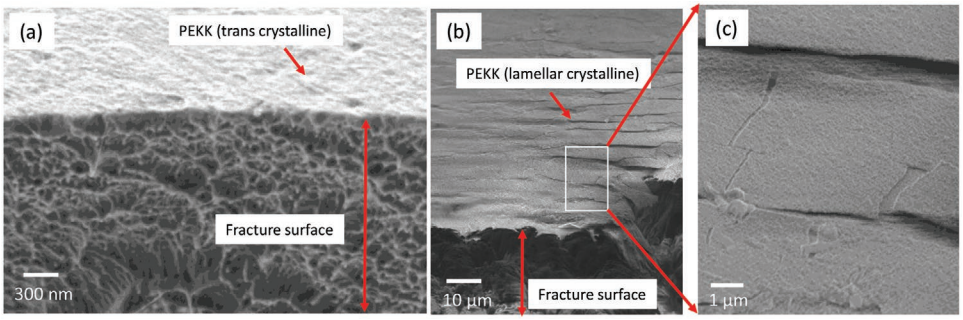

Figure 8. a) HR-SEM image of the surface and fracture surface morphology of a PEKK film with a trans-crystalline structure at the top surface. b) HR-SEM image of the surface and fracture surface morphology of a PEKK film with a lamellar crystalline structure at the top surface. c) High-resolution image of the area marked with a white square in b).

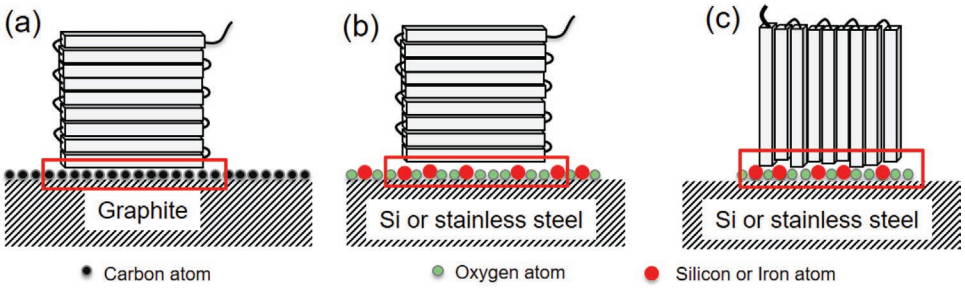

Figure 9. a) Schematic drawing of the trans-crystalline structure formed on a graphite surface. b) Schematic drawing of the trans-crystalline structure formed on a silicon wafer or a stainless steel surface. c) Schematic drawing of the lamellar crystalline structure formed on a silicon wafer or a stainless steel surface. All subfigures show the atomic arrangement at the substrate interface.

graphite or graphene-coated surfaces, the surface is composed of carbon atoms with high lattice periodicity (a hexagonal honeycomb lattice, with a bond length of 0.142 nm) as schematically shown in Figure 8a.[20] Due to the high lattice matching between the polymer chains (C—C bond length of 0.154 nm and C=C bond length of 0.134 nm) and the substrate, the graphite surface has a high nucleating ability.[21] For the stainless steel and silicon wafer surface with a native oxidized layer, the surface has an amorphous structure composed of Fe, Cr, and oxygen or Si and oxygen atoms as schematically shown in Figure 8b,c (Fe—O bond length of 0.215 nm, Cr—O bond length of 0.209 nm and 0.193 nm, and Si—O bond length of 0.165 nm).[22] A hypothesis is proposed to explain the formation of the flat-on lamellar crystal at the contact with a stainless steel surface or a silicon wafer surface. Figure 9b,c shows the schematic drawing of a trans-crystal and a flat-on lamellar crystal in contact with an amorphous substrate structure. For an amorphous substrate surface, because of the mismatching of the atomic lattice between polymer chains and the substrate surface, the free energy at the interface between the trans-crystal and the substrate is high. Thus, the trans-crystal will not form on an amorphous surface. For a flat-on lamellar crystal, because of the optimization of the chain packaging geometry at the polymer and substrate interface as shown in Figure 8c, the free energy at the interface can be further minimized. Thus, a flat-on lamellar crystal forms at the contact with an amorphous surface.

The formation of the flat-on lamellar crystals of various semicrystalline polymers on stainless steel and silicon wafer surface is reported. These results indicate that the flat-on lamellar crystals form without the presence of a nanoscale confinement. It is demonstrated that the surface physicochemical properties of the substrates also play an important role in the formation of such flat-on lamellar crystals. A hypothesis is proposed to explain the formation of the flat-on lamellar crystals based on the lattice matching between polymer crystals and the substrate. Our results are crucial for a fundamental understanding of the formation of lamellar crystals and may give a guide to the development of new approaches to purposely create or avoid such structures.

Acknowledgements

The authors acknowledge Dr. S. Wijskamp from ThermoPlastic composites Research Center (TPRC), Dr. Yibo Su, Dr. Ali Rezaei, and Dr. M. R. S. Huisman from Brightlands Materials Center (BMC) for help with materials selection. The authors acknowledge Dr. M. A. Smithers from Mesa+ Institute for help with HR-SEM characterizations.

Conflict of Interest

The authors declare no conflict of interest.

Data Availability Statement

The data that support the findings of this study are available from the corresponding author upon reasonable request.

Keywords

atomic force microscopy, heterogeneous crystallization, lamellar crystals, lattice matching, trans-crystalline structures

Received: October 29, 2020
Revised: January 26, 2021
Published online:

[1] a) F. C. Frank, M. Tosi, *Proc. R. Soc. London Ser. A* **1961**, *263*, 323; b) K. Armitstead, G. Goldbeck-Wood, A. Keller, in *Macromolecules: Synthesis, Order and Advanced Properties*, Springer, Berlin **1992**, p. 219; c) G. Reiter, G. R. Strobl, *Progress in Understanding of Polymer Crystallization*, Vol. *714*, Springer, Berlin **2007**.

[2] a) Y.-L. Loo, R. A. Register, A. J. Ryan, G. T. Dee, *Macromolecules* **2001**, *34*, 8968; b) R. M. Michell, A. J. Mueller, *Prog. Polym. Sci.* **2016**, *54*, 183; c) H. Wang, J. K. Keum, A. Hiltner, E. Baer, *Macromolecules* **2010**, *43*, 3359.

[3] a) H. Wang, J. K. Keum, A. Hiltner, E. Baer, B. Freeman, A. Rozanski, A. Galeski, *Science* **2009**, *323*, 757; b) S. Goffri, C. Müller, N. Stingelin-Stutzmann, D. W. Breiby, C. P. Radano, J. W. Andreasen, R. Thompson, R. A. Janssen, M. M. Nielsen, P. Smith, *Nat. Mater.* **2006**, *5*, 950; c) T. V. Duncan, *J. Colloid Interface Sci.* **2011**, *363*, 1; d) H. Wang, J. K. Keum, A. Hiltner, E. Baer, *Macromolecules* **2009**, *42*, 7055; e) J. M. Carr, D. S. Langhe, M. T. Ponting, A. Hiltner, E. Baer, *J. Mater. Res.* **2012**, *27*, 1326.

[4] M. Heshmati, R. Haghani, M. Al-Emrani, *Composites, Part B* **2015**, *81*, 259.

[5] M. Müller, *Polymer Science: A Comprehensive Reference*, Vol. *1* (Eds: K. Matyjaszewski, M. Muller), Elsevier BV, Amsterdam **2012**, p. 387.

[6] a) R.-M. Ho, F.-H. Lin, C.-C. Tsai, C.-C. Lin, B.-T. Ko, B. S. Hsiao, I. Sics, *Macromolecules* **2004**, *37*, 5985; b) Y.-L. Loo,

R. A. Register, A. J. Ryan, *Macromolecules* **2002**, *35*, 2365; c) W. Lee, H. L. Chen, T. L. Lin, *J. Polym. Sci. Part B: Polym. Phys.* **2002**, *40*, 519; d) D. J. Quiram, R. A. Register, G. R. Marchand, D. H. Adamson, *Macromolecules* **1998**, *31*, 4891; e) C. Göbel, C. Hils, M. Drechsler, D. Baabe, A. Greiner, H. Schmalz, B. Weber, *Angew. Chem., Int. Ed.* **2020**, *59*, 5765; f) R. Dehmel, J. A. Dolan, Y. Gu, U. Wiesner, T. D. Wilkinson, J. J. Baumberg, U. Steiner, B. D. Wilts, I. Gunkel, *Macromolecules* **2017**, *50*, 6255; g) E. C. Davidson, R. A. Segalman, *Macromolecules* **2017**, *50*, 8097; h) L. Zha, W. Hu, *Prog. Polym. Sci.* **2016**, *54*, 232.

[7] a) G. Reiter, J.-U. Sommer, *Phys. Rev. Lett.* **1998**, *80*, 3771; b) G. Reiter, J.-U. Sommer, *J. Chem. Phys.* **2000**, *112*, 4376; c) J.-U. Sommer, G. Reiter, *J. Chem. Phys.* **2000**, *112*, 4384; d) F. Zhang, J. Liu, H. Huang, B. Du, T. He, *Eur. Phys. J. E* **2002**, *8*, 289; e) Y. Sakai, M. Imai, K. Kaji, M. Tsuji, *J. Cryst. Growth* **1999**, *203*, 244.

[8] a) H. Abe, Y. Kikkawa, T. Iwata, H. Aoki, T. Akehata, Y. Doi, *Polymer* **2000**, *41*, 867; b) A. J. Kovacs, C. Straupe, *Faraday Discuss. Chem. Soc.* **1979**, *68*, 225; c) A. J. Lovinger, H. Keith, *Macromolecules* **1979**, *12*, 919; d) D. E. Martínez-Tong, B. Vanroy, M. Wübbenhorst, A. Nogales, S. Napolitano, *Macromolecules* **2014**, *47*, 2354.

[9] L. Chu, W. J. B. Wouter, M. van Drongelen, Y. Guha, E. G. de Vries, R. Akkerman, M. B. de Rooij, *Adv. Eng. Mater.* **2021**, *23*, 2000518.

[10] a) H.-J. Butt, M. Jaschke, *Nanotechnology* **1995**, *6*, 1; b) L. Chu, M. Bus, A. V. Korobko, N. A. Besseling, *Ultramicroscopy* **2019**, *205*, 1.

[11] L. Gránásy, T. Pusztai, G. Tegze, J. A. Warren, J. F. Douglas, *Phys. Rev. E* **2005**, *72*, 011605.

[12] G. W. Ehrenstein, *Polymeric Materials: Structure, Properties, Applications*, Carl Hanser Verlag GmbH Co KG, Germany **2012**.

[13] B. Crist, J. M. Schultz, *Prog. Polym. Sci.* **2016**, *56*, 1.

[14] a) Q. Guan, B. Norder, L. Chu, N. A. Besseling, S. J. Picken, T. J. Dingemans, *Macromolecules* **2016**, *49*, 8549; b) L. Chu, A. V. Korobko, A. Cao, S. Sachdeva, Z. Liu, L. C. de Smet, E. J. Sudhölter, S. J. Picken, N. A. Besseling, *Adv. Mater. Interfaces* **2017**, *4*, 1600495; c) S. Magonov, V. Elings, M.-H. Whangbo, *Surf. Sci.* **1997**, *375*, L385.

[15] J. I. Lauritzen Jr., J. D. Hoffman, *J. Appl. Phys.* **1973**, *44*, 4340.

[16] a) G. Pompe, E. Mäder, *Compos. Sci. Technol.* **2000**, *60*, 2159; b) K. Cho, D. Kim, S. Yoon, *Macromolecules* **2003**, *36*, 7652.

[17] B. Wang, T. Wen, X. Zhang, A. Tercjak, X. Dong, A. J. Müller, D. Wang, D. Cavallo, *Macromolecules* **2019**, *52*, 6274.

[18] a) T. Wen, G. Liu, Y. Zhou, X. Zhang, F. Wang, H. Chen, J. Loos, D. Wang, *Macromolecules* **2012**, *45*, 5979; b) Z. Guo, S. Li, X. Liu, J. Zhang, H. Li, X. Sun, Z. Ren, S. Yan, *J. Phys. Chem. B* **2018**, *122*, 9425; c) J. Liu, J. Wang, H. Li, D. Shen, J. Zhang, Y. Ozaki, S. Yan, *J. Phys. Chem. B* **2006**, *110*, 738.

[19] a) C. Wang, L. Hwang, *J. Polym. Sci. Part B: Polym. Phys.* **1996**, *34*, 47; b) C. Wang, Y.-J. Wu, C.-Y. Fang, C.-W. Tsai, *Compos. Sci. Technol.* **2016**, *126*, 1.

[20] A. K. Geim, K. S. Novoselov, *Nanoscience and Technology: A Collection of Reviews from Nature Journals*, World Scientific, London **2010**, p. 11.

[21] C. Wang, C. Liu, *Polymer* **1997**, *38*, 4715.

[22] a) M. T. Dove, D. A. Keen, A. C. Hannon, I. P. Swainson, *Phys. Chem. Miner.* **1997**, *24*, 311; b) A. T. García-Sosa, M. Castro, *Int. J. Quantum Chem.* **2000**, *80*, 307; c) M. M. Islam, T. Couvant, P. Marcus, B. Diawara, *J. Chem.* **2017**, *2017*, 1; d) T. Ohmi, Y. Nakagawa, M. Nakamura, A. Ohki, T. Koyama, *J. Vac. Sci. Technol. A* **1996**, *14*, 2505.